Temperature Dependence of Excited-State Proton Transfer in Water Electrolyte Solutions and Water−Methanol Solutions

Pavel Leiderman, Rinat Gepshtein, Anna Uritski, Liat Genosar, and Dan Huppert*

Raymond and Beverly Sackler Faculty of Exact Sciences, School of Chemistry, Tel Aviv University, Tel Aviv 69978, Israel

Received: February 27, 2006; In Final Form: May 10, 2006

The reversible proton dissociation and geminate recombination of a photoacid is studied as a function of temperature in water electrolyte solutions and binary water−methanol mixtures, containing 0.1 and 0.2 mole fractions of methanol. 8-Hydroxypyrene-1,3,6-trisulfonate trisodium salt (HPTS) is used as the photoacid. The experimental data are analyzed by the reversible geminate recombination model. We found that the slope of the logarithm of the proton-transfer rate constant as a function of the inverse of temperature (Arrhenius plot) in the liquid phase of these samples are temperature-dependent, while in the solid phase, the slope is nearly constant. The slope of the Arrhenius plot in frozen electrolyte solution is larger than that of the water−methanol mixtures, which is about the same as in pure water. Careful examination of the time-resolved emission in ice samples shows that the fit quality using the geminate recombination model is rather poor at relatively short times. We were able to get a better fit using an inhomogeneous kinetics model assuming the proton-transfer rate consists of a distribution of rates. The model is consistent with an inhomogeneous frozen water distribution next to the photoacid.

Introduction

Proton-transfer reactions are common in chemical and biological processes.[1−4] Over the last two decades, intermolecular proton transfer in the excited state (ESPT) has been studied extensively and provided pertinent information about the mechanism and the parameters controlling acid−base reactions.[5−12]

To initiate these reactions, protic solvent solutions of a photoacids are irradiated by short (femtosecond−picosecond) laser pulses.[13−15] Consequently, the excited-state molecules dissociate very rapidly by transferring a proton to a nearby solvent molecule. 8-Hydroxypyrene-1,3,6-trisulfonate (HPTS or pyranine) is a photoacid commonly used in the study of ESPT process.[15−17] The excited-state deprotonated form RO^-* is quadruply negatively charged. Thus, the reversible geminate recombination process is strongly enhanced relative to a singly charged photoacid like 2-naphthol. The proton-transfer rate could be determined either by the initial decay time of the time-resolved fluorescence of the protonated form (ROH*) measured at 440 nm or by the slow rise time of the emission of the deprotonated species (RO^-*) at about 520 nm.

Over the past decade, we have used a model for an intermolecular ESPT process that accounts for the geminate recombination of the transferred proton. We describe briefly the model in a separate subsection.

Two decades ago, we studied the rate of proton transfer from photoacids to the solvent in concentrated aqueous solutions (1−6 M) of strong electrolytes[18] (LiBr, $LiC1O_4$, NaC1, NaClO, KCl, $MgC1_2$, $MgC1O_4$). The rate of dissociation decreases upon increasing the concentration of the salt. Results obtained with different salts fit a single straight line when the log of the rate constant is drawn versus the log of water activity. It was proposed[18] that the rate of proton dissociation is related to the free energy of proton hydrate formation.

In a recent study,[19] we followed our work of the salt effect on the ESPT process in aqueous concentrated salt solutions conducted more than two decades ago.[18] The main finding of this study[19] is that, at high concentrations of $MgCl_2$, $c > 2$ M, the time-resolved fluorescence decay of the photoacid, ROH, is nonexponential even at much shorter times than the inverse of the proton-transfer rate, $t \leq 1/k_{PT}$, where k_{PT} is the proton-transfer rate constant ($1/k_{PT} \approx 100$ ps in pure water and about 350 ps at 2 M $MgCl_2$). Over this short time range, the reversible geminate recombination model predicts nearly exponential decay, especially when the Coulomb potential is almost totally screened by the salt ions. We explained the surprising experimental findings by the proton-transfer rate in a concentrated salt solution not having a single value (exponential decay) but rather a distribution of rates arising from the distribution of the microenvironment next to the HPTS. Hence, the measured proton-transfer rate is nonexponential.

In this study, we extended the previous study[19] and conducted time-resolved emission measurements of HPTS in an electrolyte solution, not only at room temperature but over a wide range of temperatures. We extensively studied the temperature dependence of the reversible protolytic process in a pure aqueous solution and in ice.[20] It was found that the proton-transfer rate constant, k_{PT}, is almost temperature-independent at high temperatures, $T > 280$ K. At lower temperatures, the dependence of k_{PT} on the temperature increases. The activation energy of k_{PT} is temperature-dependent. It is low, $E_a < 8$ kJ/mol, in the high-temperature region, and at about 269 K, it is almost 20 kJ/mol. In the ice phase, the activation energy is nearly constant down to about 240 K, $E_a \approx 30$ kJ/mol.

* Corresponding author. Dan Huppert. E-mail: huppert@tulip.tau.ac.il. Phone: 972-3-6407012. Fax: 972-3-6407491.

10.1021/jp061226c CCC: $33.50
Published on Web 07/06/2006

In this study, we found that, in an electrolyte solution, the temperature dependence of k_{PT} in the liquid phase is about the same as in pure water. In the ice phase, the activation energy increases twofold, $E_a \approx 60$ kJ/mol. We also studied the temperature dependence of the ESPT process in water-rich water−methanol mixtures. The freezing point of a water−methanol mixture of $\chi_{CH_3OH} = 0.2$ is 243 K.[21] This enabled us to extend the measurements in the liquid state by about 30 °C. The reversible geminate recombination model nicely fits the time-resolved emission of a solution of $\chi_{CH_3OH} = 0.2$ from 330 K to the freezing point at 243 K. The activation energy increases as the temperature decreases, in a manner similar to that of pure water (which can be followed in pure water only to about 273 K). We found that the activation energies of k_{PT} in the frozen samples are somewhat smaller than that of pure ice, $E_a \approx 28$ kJ/mol. The activation energies in the liquid and solid phases, at the freezing point (243 K), are about the same.

Experimental Section

Time-resolved fluorescence was acquired using the time-correlated single-photon counting (TCSPC) technique, the method of choice when sensitivity, a large dynamic range, and low-intensity illumination are important criteria in fluorescence decay measurements.

For excitation, we used a cavity-dumped Ti:sapphire femtosecond laser, Mira, Coherent, which provides short, 80 fs, pulses of variable repetition rate, operating at the second harmonic generation (SHG) frequency, over the spectral range 380−400 nm with the relatively low repetition rate of 500 kHz. The TCSPC detection system is based on a Hamamatsu 3809U photomultiplier and Edinburgh Instruments TCC 900 computer module for TCSPC. The overall instrumental response was about 35 ps (fwhm). Measurements were taken at 10 nm spectral width. The observed transient fluorescence signal, $I(t)$, is a convolution of the instrument response function (IRF), $I_0(t)$, with the theoretical decay function. The excitation pulse energy was reduced by neutral density filters to about 10 pJ. We checked the sample's absorption prior to and after time-resolved measurements. We could not find noticeable changes in the absorption spectra due to sample irradiation.

Steady-state fluorescence spectra were taken using a FluoroMax (Jobin Yvon) spectrofluorimeter. The HPTS, of laser grade, was purchased from Kodak or Aldrich. $MgCl_2$ and NaCl (analytical grade) were purchased from Aldrich. Perchloric acid, 70% reagent grade, was purchased from Aldrich. For steady-state fluorescence measurements, we used solutions of $\sim 2 \times 10^{-5}$ M of HPTS. The sample concentrations were between 2×10^{-4} and 2×10^{-5} M. Deionized water had resistance of >10 MΩ. Methanol, of analytical grade, was from BDH. All chemicals were used without further purification. The solution pH was about 6.

The HPTS fluorescence spectrum consists of two structureless broad bands (~40 nm fwhm). The emission band maximum of the acidic form (ROH*) and the alkaline form (RO^-*) in water are at 440 and 512 nm, respectively. The contribution of the RO^-* band to the total intensity at 435 nm is less than 0.2%. To avoid overlap between contributions of the two species, we mainly monitored the ROH* fluorescence at 435 nm.

The temperature of the irradiated sample was controlled by placing the sample in a liquid N_2 cryostat with a thermal stability of approximately ±1.5 K.

Reversible Diffusion-Influenced Two-Step Proton-Transfer Model. In this model,[12,16,17] the overall dissociation process can be subdivided into the two consecutive steps of reaction and diffusion. In the reactive stage, a rapid short-range charge separation occurs, and a solvent-stabilized ion pair is formed. This is followed by a diffusive stage, when the two ions withdraw from each other due to their thermal random motion. The reverse process is a geminate recombination (neutralization) of the two separated ions either by the direct collapse of the ion pair or by following a geminate reencounter of the solvated "free" ions.

Mathematically, one considers the probability density, $p(r, t)$, for the pair to separate to a distance r by time t after excitation. The observed (normalized) signals from the excited acid and anion correspond to the protonation probability, $P(t)$, and the survival probability of the separated pair

$$S(t) \equiv 4\pi \int_a^\infty p(r, t) r^2 \, dr \tag{1a}$$

$$P(t) = 1 - S(t) \tag{1b}$$

The separated pair at time t, $p(r, t)$, is assumed to obey a spherically symmetric Debye−Smoluchowski equation (DSE) in three dimensions (eq 2a) which is coupled to a kinetic equation for $P(t)$ (eq 2b) which serves as the boundary condition for the differential eq 2a.[12]

$$\frac{\partial p(r, t)}{\partial t} = \left[r^{-2} \frac{\partial}{\partial r} D r^2 \, e^{-V(r)} \frac{\partial}{\partial r} e^{V(r)} - k_0'\right] p(r, t) + [k_{PT} P(t) - k_r p(r, t)] \frac{\delta(r - a)}{4\pi a^2} \tag{2a}$$

$$\frac{\partial}{\partial t} P(t) = k_r p(a, t) - (k_{PT} + k_0) P(t) \tag{2b}$$

where a is the contact radius, and k_{PT} and k_r are the proton-transfer and recombination rate constants, respectively.

The geminate recombination is given by a δ function "sink term", $k_r \delta(r - a)/(4\pi a^2)$. In contrast, the ROH* and RO^-* radiative decay rate constants (k_0 and k_0', respectively) are r-independent. The radiative rate of ROH^* is determined in the absence of an excited-state proton-transfer reaction (measured in neat methanol solution). When the proton reaches the reaction sphere at $r = a$, it recombines geminately to reform ROH* with a rate constant k_r (reflective boundary condition). The mutual attraction of the proton and the HPTS anion is described by a distance-dependent potential, $V(r)$, in units of the thermal energy $k_B T$. In this study, the ESPT process is examined in the presence of a large salt concentration in an aqueous solution. We therefore apply the screened Coulomb potential of Debye and Hickel[22]

$$V(r) = -\frac{R_D}{r} \frac{\exp[-\kappa_{DH}(r - a)]}{1 + \kappa_{DH} a} \tag{3}$$

where R_D and κ_{DH}^{-1} are the Debye and ionic-atmosphere radii, respectively, and a is its ionic radius.

$$R_D \equiv \frac{|z_1 z_2| e^2}{\epsilon k_B T}$$

$$\kappa_{DH}^2 \equiv \frac{8\pi e^2 c}{\epsilon_s k_B T}$$

$$\kappa_{DH} \equiv A\sqrt{c} \tag{4}$$

$z_1 = 1$ and $z_2 = -4$ are the charges of the proton and the deprotonated HPTS, respectively. e is the electronic charge, ϵ_s

is the static dielectric constant of the solvent, k_B is Boltzmann's constant, T is the absolute temperature, and c is the concentration of the electrolyte.

The relative diffusion constant, D, is the sum of the protic and anionic diffusion coefficients. Since the proton is abnormally fast, whereas the anion is bulky and slow, its diffusion coefficient may be neglected with respect to that of the proton. We do not employ any distance dependence in D, mainly because procedures for doing so are not well-established.

As compared with traditional treatments of diffusion-influenced reactions,[23] the new aspect is the reversibility of the reaction, described by the "back-reaction" boundary condition.[17,24,25] The process we wish to consider begins upon photochemical excitation, which prepares a thermally and vibrationally equilibrated ROH* acidic form in the lowest excited electronic state, S_1. Thus, the initial condition is

$$P(0) = 1 \quad p(r, 0) = 0 \tag{5}$$

where $P(0)$ denotes the excited-state ROH probability at $t = 0$.

The bound and dissociated states evolve according to eq 2a with boundary condition set by eq 2b. We solve these equations numerically using the Windows application[26] for solving the spherically symmetric diffusion problem (SSDP), convolute $P(t)$ with the IRF, and compare it with the ROH* fluorescence signal.

The asymptotic expression (the long-time behavior) for the fluorescence of ROH* in the case where both forms of the photoacid, ROH and RO^-, have the same lifetime is given by[25]

$$[\mathrm{ROH}^*] \exp[t/\tau_f] \cong \frac{\pi}{2} a^2 \{\exp[V(a)]\} \frac{k_r}{k_{PT}(\pi D)^{3/2}} t^{-d/2} \tag{6}$$

where τ_f is the excited-state lifetime of both the protonated form, ROH, and the deprotonated form, RO^-, and d is the dimensionality of the relevant problem. All other symbols are as previously defined. Equation 6 shows that the tail amplitude depends on several parameters, but its time dependence is a power law of time that depends on the dimensionality of the problem. For three dimensions, it assumes the power law of $t^{-3/2}$.

GR Model-Fitting Procedure and Treatment of the Adjustable Parameters. k_{PT} determines the initial slope of the decay curves: the larger the k_{PT} is, the faster the initial exponential drop. The intrinsic recombination rate constant, k_r, almost does not affect the behavior at $t \rightarrow 0$ but determines the magnitude of the long-time tail. The effect of increasing k_r is somewhat similar to decreasing D. It differs from the effect of changing R_D or a in the curvature of these plots. The parameters for the numerical solution of the DSE were taken from the literature.[22,27] The contact radius $a = 6$ Å is slightly larger than the molecule's spherical gyration radius (4.5−5.5 Å), obtained from measurements of HPTS rotation times.[28] It probably accounts for at least one layer of water molecules around the HPTS anion. All the above-mentioned parameters, except the contact radius a, are temperature-dependent. The temperature dependence of $D(T)$ and $\epsilon_s(T)$ of pure water in the liquid and supercooled liquid are given in the literature.[25,29−33]

At room temperature and neat water, there are only two free adjustable parameters in solving and fitting the experimental data, the proton-transfer rate, k_{PT}, and the recombination rate, k_r. The literature only covers the proton conductance in the liquid phase as a function of temperature in neat water solution. In general, the effect of salt on the proton conductance is a reduction of the proton conductance with salt concentration.[25] Thus, the diffusion constant, D_{H+}, is known only in limited cases (most of the data are measured at about 295 K), which do not include the particular salt solutions or the water−methanol mixtures used in this study. We are unaware of published data for the proton diffusion constant at the low-temperature liquid range and in the ice phase in these samples. Thus, $D(T)$ in most of the temperature range studied is a free adjustable parameter in our model calculations. It is determined by the best fit to the time-resolved emission signal of ROH. To summarize, when D_{H+} is known from independent measurements (conductance), the two free fitting parameters are k_{PT} and k_r. In most of the experimental data represented in this study, $D_{H+}(T)$ is unknown, and thus, D_{H+} is an additional adjustable parameter which we chose by best fit and the knowledge of its values in similar systems or at other temperatures. In general, if $k_{PT} > k_r$ and D is small, $D \leq 10^{-5}$ cm^2/s, then the value of k_{PT} mainly controls the initial decay of ROH at short times. Once k_{PT} is approximately determined, k_r and D control the amplitude of the longer times. k_r affects strongly the shape and amplitude of the intermediate times $1/k_{PT} < t < 3/k_r$. Once k_r is determined, D is the only parameter left to control the amplitude of the long times of the emission curve of the ROH.

The absolute fluorescence quantum yield of ROH is given by

$$\Phi(\mathrm{ROH}^*) = \tau_f^{-1} \int_0^\infty P(t) \exp -t/\tau_f \, dt \tag{7}$$

Inhomogeneous Proton-Transfer Kinetics Model for Ice Samples. In recent papers,[19,34] we used a model that accounts for inhomogeneous kinetics that arises from a frozen structural media surrounding an ensemble of excited molecules. The model is applicable only in very viscous solvents or frozen matrixes when no structural relaxation takes place during the excited-state lifetime. We wish to use the model to fit the proton-transfer ice data. In ice, most of the water molecules are immobile. Only a few water molecules, at the defect point, can rotate.[35] We assume that the water next to the HPTS molecule or near an ion is in a frozen disordered structure. An inhomogeneous frozen water model accounts for a distribution of proton-transfer rates, which strongly affects the time-resolved emission of the ROH of a photoacid.

The mathematical derivation of the inhomogeneous kinetics model in ice is similar to that of ref 34, which deals with the radiationless transition of the GFP chromophore in solution. In the proposed model, we assume that the proton is transferred to a water cluster next to the hydroxyl group of HPTS. For simplicity, we assume that the inhomogeneous distribution of the ice structure next to HPTS is Gaussian with a certain width defined by a variance σ and an average structure x_0. We shall use a continuous coordinate x ($x \geq 0$) to define the distribution. The distribution is given by

$$p(x) = \frac{1}{\sqrt{2\pi\sigma^2}} \exp\left[-\frac{(x - x_0)^2}{2\sigma^2}\right] \tag{8}$$

where x_0 is the mean (the peak position) of the Gaussian. We assume that the rate constant of proton transfer depends exponentially on the coordinate x. The Gaussian position is set at $x_0 = 1.5$ such that the rate constant at room temperature assumes the value of a neat water solution (for HPTS, $k_{PT} \approx 10$ ns^{-1}). The larger the value of x is, the smaller the proton-transfer rate. The rate constant is given by

$$k(x) = A \exp -[x] \tag{9}$$

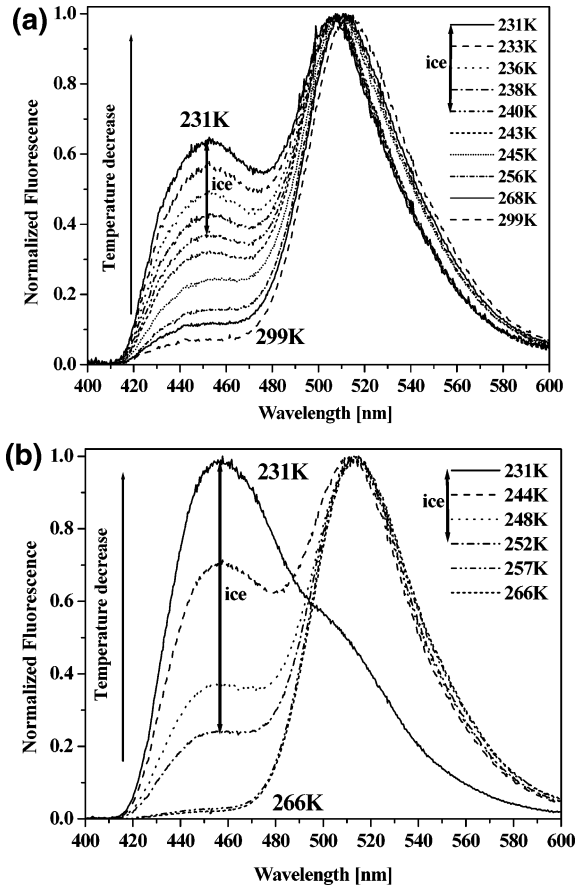

Figure 1. Steady-state emission of HPTS in the liquid and solid phases excited at 400 nm at several temperatures. (a) Water−methanol solution of 40 vol % methanol (b) Aqueous solution containing 0.35 M $MgCl_2$.

The temperature dependence of the proton-transfer rate constant in ice is given by the activation energy relation

$$A = A_0 \exp{-\left(\frac{E_a}{RT}\right)} \tag{10}$$

In the static limit, where the ice structure next to the hydroxyl group of HPTS is time-independent with respect to the time of the proton-transfer rate, the probability $P(t)$ that the excited state has not transferred a proton by the time t after excitation is given by

$$P(t) = \exp\left(\frac{-t}{\tau_f}\right) \int_0^\infty p(x) \exp[-k(x)t]\, dx \tag{11}$$

The first exponential accounts for the homogeneous radiative decay process, whereas the integral of the second exponential represents the inhomogeneous proton-transfer rate that depends on the ice structure. The decay of $P(t)$ is nonexponential and depends on the mean value $k(x_0)$ and the Gaussian width $2\sigma^2$.

Results

Steady-State Emission. Figure 1a shows the steady-state emission of an HPTS water−methanol solution of 40 vol % methanol ($\chi_{CH_3OH} = 0.2$) excited at 400 nm and measured at several temperatures in the range 230−300 K. At high temperatures, the intensity of the ROH emission (peak position at 445 nm) is relatively small, <5% of the intense green emission of the RO^- (peak position 515 nm). As the temperature decreases, the ROH emission intensity increases. In ice like samples (frozen samples), $T < 243$ K, the intensity of the ROH band increases rapidly with temperature. Figure 1b shows similar results of an aqueous solution containing 0.35 M $MgCl_2$. The sample freezing point is at about 267 K. The temperature dependence of the position, the bandwidth, and the shape of both bands is small in the liquid and solid phases.

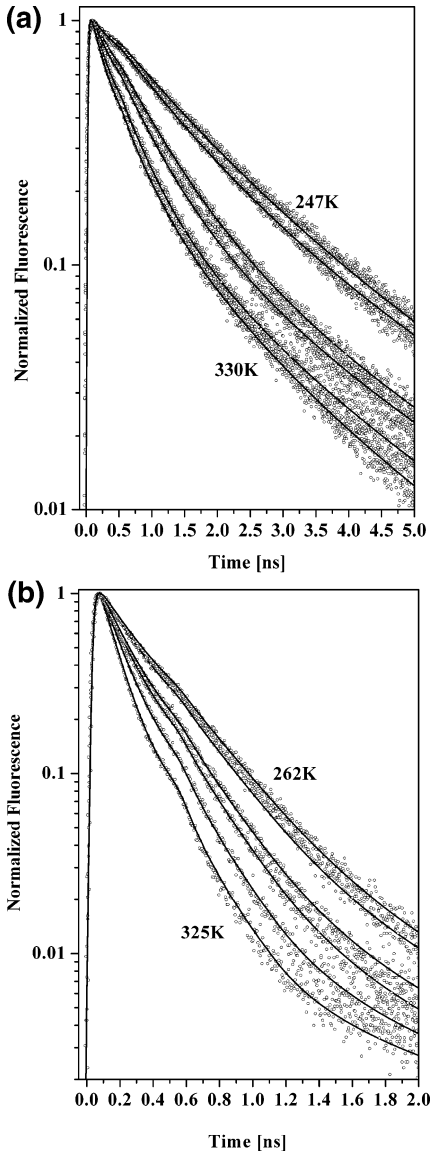

Figure 2. Time-resolved emission of the ROH band of HPTS measured at 435 nm at several temperatures. Circles, experimental results; solid line, the computer fit to the geminate recombination model. (a) 40 vol % methanol liquid water−methanol solution. (b) 1 M $MgCl_2$ liquid solution.

Time-Resolved Emission. Figure 2a shows the time-resolved emission of the ROH band of HPTS at 435 nm of a sample of $\chi_{CH_3OH} = 0.2$ methanol liquid solution at several temperatures in the range 247−330 K. Along with the experimental data, we also show a computer fit (solid line), computed according to the reversible geminate recombination model. The initial slope, measured at the early times after the instrument's response (about 30 ps) of the various decay curves, provides the proton-transfer rate. The long-time nonexponential tail strongly depends on the proton recombination rate, the diffusion constant, and the Coulomb attraction between the proton and the RO^-*. As the temperature decreases, the fitting parameters k_{PT}, k_r, and D also decrease. The fitting parameters for neat water solutions are given in Table 1. Figure 2b shows the time-resolved emission of the ROH band of HPTS at 435 nm of a sample of a 1 M

TABLE 1: Temperature Dependence of the Geminate Recombination Model Parameters for the Proton-Transfer Reaction of HPTS in H_2O

T [K]	k_{PT}[a] [10^9 s^{-1}]	k_r[a,b] [10^9 Å s^{-1}]	D [cm^2 s^{-1}]
354	9.9	10.8	1.9×10^{-4} [c]
343	9.6	7.5	1.4×10^{-4} [c]
309	9.3	5.1	1.1×10^{-4} [c]
295	8.8	5.0	8.7×10^{-5} [c]
288	7.9	3.3	6.0×10^{-5} [c]
278	6.8	3.0	5.6×10^{-5} [c]
275	6.3	2.6	5.3×10^{-5} [c]
274	6.0	2.5	5.2×10^{-5} [c]
271	5.6	2.2	4.8×10^{-5} [c]
268	5.3	2.1	4.6×10^{-5}
267[d]	2.6	2.5	4.4×10^{-5} [e]
266[d]	2.2	2.4	4.2×10^{-5} [e]
263[d]	1.4	2.1	4.0×10^{-5} [e]
260[d]	0.98	2.1	3.6×10^{-5} [e]
256[d]	0.65	1.50	3.1×10^{-5} [e]
251[d]	0.43	1.45	2.1×10^{-5}[e]

[a] k_{PT} and k_r are obtained from the fit of the experimental data by the reversible proton-transfer model (see text) $\tau_{ROH}^{-1} = 0.18$ ns^{-1}, $\tau_{RO^-}^{-1} = 0.19$ ns^{-1}. [b] The error in the determination of k_r is 50%; see text. [c] Calculated from the data of ref 31. [d] Ice samples. [e] Estimated from best fit.

$MgCl_2$ liquid solution at several temperatures in the range 262−325 K. As seen in Figure 2, the fits to the decay curves in the liquid state are rather good at all temperatures.

In the frozen phase, the change in the proton-transfer rate constant with temperature is larger than at high temperatures in the liquid state. A similar effect is observed in the steady-state emission (shown in Figure 1), where, in the ice phase, the intensity of the ROH band strongly increases with the temperature decrease. The RO^- band intensity decreases with the temperature decrease. Figure 3a,b shows the time-resolved emission of the ROH band in the ice phase, at several temperatures of an $\chi_{CH_3OH} = 0.2$ solution and a 1 M $MgCl_2$ solution, respectively, along with the computer fit (solid line) using the geminate recombination model. In the ice phase, the quality of the fit decreases somewhat from that of a high-temperature liquid.

Figure 4 shows the time-resolved emission of the RO^- band measured at 515 nm for an aqueous solution containing 1 M of $MgCl_2$ at several temperatures. The lower the temperature is, the longer the rise time of the signal. At a specific temperature, the rise time of the RO^- signal nicely fits the decay rate of the ROH signal. The solid line is the computer fit using the proton-transfer model with the parameters used to fit the ROH signal (see Figure 2b and Table 2). Thus, we simultaneously fit, with the same fitting parameters, the time-resolved emission of both ROH and RO^-. In the case of the RO^- signal, we get a good fit when we assume an overlap of the ROH and RO^- spectral bands. The signal of RO^-, measured at about the peak (515 nm), consists of the relative signals of about 0.2 and 0.8 of ROH and RO^- emission, respectively. This overlap of the bands is larger by about 35% than that estimated from the overlap of the two steady-state emission bands.[36]

Discussion

In this study, we measured the proton-transfer and geminate recombination rates of HPTS as a function of temperature in liquid water containing $MgCl_2$ and NaCl and in water−methanol solutions. We also measured these rates in the solid phase.

In the solid phase, the photoacid tends to "salt out" the HPTS, and as a consequence, the luminescence intensity in frozen samples strongly reduces. The net result is unreliable time-resolved emission measurements in the ice phase, of both the acid and base forms. The "salting out" problem of HPTS out of the ice phase was not noticed at all salt concentrations or water−methanol solvent mixture compositions. In methanol−water mixtures, the freezing point lowers as the methanol mole fraction increases. At $\chi_{CH_3OH} = 0.2$, the freezing point is 243 K. This offered us the opportunity to extend the previous study of the ESPT process in the liquid phase to a much lower temperature.

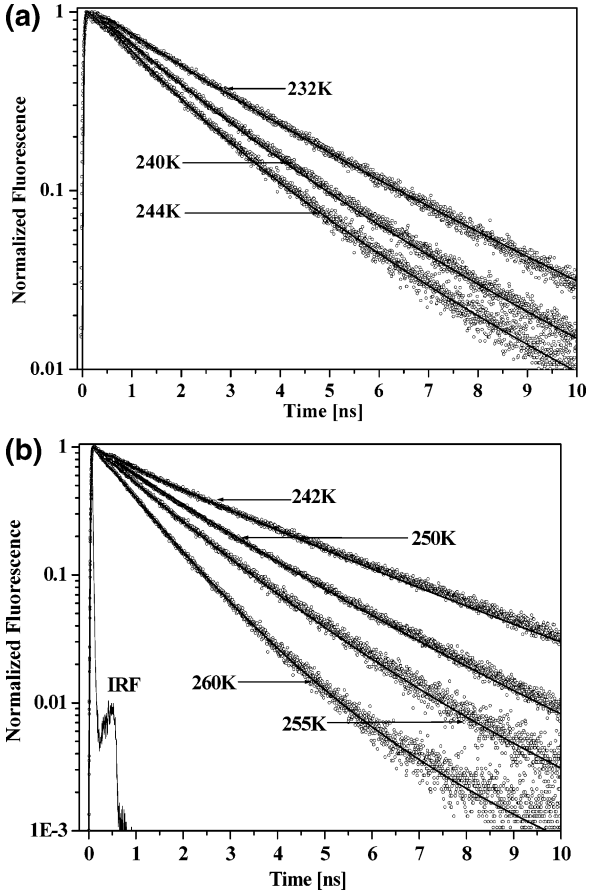

Figure 3. Time-resolved emission of the ROH band of HPTS in the ice phase, measured at 435 nm at several temperatures. Symbols, experimental results; solid line, the computer fit to the geminate recombination model. (a) 40 vol % methanol liquid water−methanol solution. (b) 1 M $MgCl_2$ liquid solution.

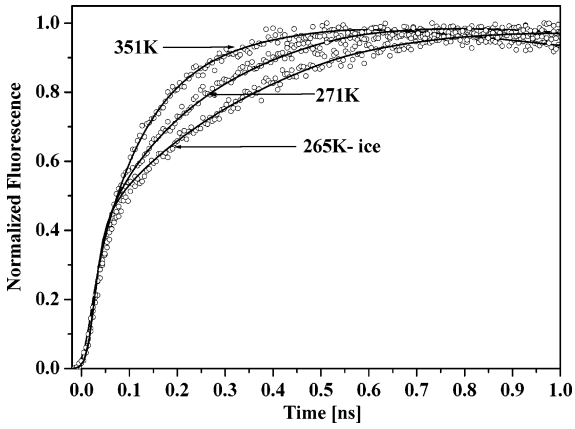

Figure 4. Time-resolved emission of the RO^- band measured at 515 nm for an aqueous solution containing 1 M of $MgCl_2$ at several temperatures. Symbols, experimental results; solid line, the computer fit to the geminate recombination model.

TABLE 2: Temperature Dependence of the Geminate Recombination Model Parameters for the Proton-Transfer Reaction of HPTS in a 1 M $MgCl_2/H_2O$ Solution

T [K]	k_{PT}[a] [10^9 s^{-1}]	k_r[a,b] [10^9 Å s^{-1}]	D[c] [cm^2 s^{-1}]
349	8.6	6.9	4.0×10^{-5}
337	8.3	6.3	3.5×10^{-5}
325	8.1	6.2	3.1×10^{-5}
315	7.7	6.0	2.8×10^{-5}
304	7.1	5.8	2.5×10^{-5}
296	6.5	5.6	2.3×10^{-5} [e]
290	6.2	5.5	2.2×10^{-5}
283	5.8	5.4	2.1×10^{-5}
281	5.3	5.2	2.0×10^{-5}
279	5.2	5.1	1.9×10^{-5}
275	4.9	5.0	1.8×10^{-5}
271[d]	4.3	4.8	1.7×10^{-5}
267[d]	3.7	2.5	9.5×10^{-6}
262[d]	1.5	2.3	7.5×10^{-6}
260[d]	0.97	1.0	4.0×10^{-6}
257[d]	0.77	0.90	3.0×10^{-6}
255[d]	0.63	0.80	2.5×10^{-6}
250[d]	0.43	0.68	2.0×10^{-6}
247[d]	0.34	0.67	1.4×10^{-6}
242[d]	0.27	0.67	1.1×10^{-6}
239[d]	0.22	0.65	1.1×10^{-6}

[a] k_{PT} and k_r are obtained from the fit of the experimental data by the reversible proton-transfer model (see text). [b] The error in the determination of k_r is 50%; see text. [c] Values of D obtained by best fit to the fluorescence decay. [d] Ice samples. [e] Taken from ref 19.

Proton Transfer in Liquid Water−Salt Solutions. In a recent work,[19] we studied the effect of strong electrolytes on the proton-transfer rates of HPTS. The proton-transfer rate constant to pure water solution, $k_{PT} \approx 10$ ns^{-1}, is almost independent of the electrolyte concentration in the low salt concentration range of about <1 M $MgCl_2$. The Mg^{2+} ion was found to strongly influence the rate of proton transfer especially in the large concentration range $c > 1.5$ M. At about 5 M $MgCl_2$, the proton-transfer rate constant is smaller than the radiative rate, $k_{rad} \approx 0.2$ ns^{-1}, and hence, the proton-transfer quantum efficiency is very small, $\Phi_{PT} < 0.05$, compared with about $\Phi_{PT} \approx 0.97$ in pure water. In an aqueous solution of about 6 M NaCl, the rate reduces by only a factor of 3, and the ESPT quantum efficiency is effectively unchanged.

We explained the strong Mg^{2+} effect on the ESPT rate by the reduction of the fraction of free water molecules, due to the large number of water molecules that are bound in the solvation layers of Mg^{2+}. Hasted and co-workers[37] studied the dielectric constant depression of aqueous solutions containing electrolytes. They related the depression of the static dielectric constant with the number of water molecules needed to solvate the various ions. They calculated the number of water molecules solvating Mg^{2+}, H_3O^+, and Na^+ to be 14, 10, and 4, respectively. For large concentrations of Mg^{2+} ($c \geq 1.5$ M), the available fraction of unbound water molecules strongly decreases, and hence, the free water that is essential for the efficient excited-state proton transfer decreases as the salt concentration increases. The overall effect is a large dependence of the proton-transfer rate constant on Mg^{2+} concentrations.

Figure 5a−c shows an Arrhenius plot of the logarithm of the proton-transfer rate constant of HPTS, $\ln(k_{PT})$ vs $1/T$, in pure water and in solutions containing several concentrations of $MgCl_2$ and NaCl. In all these solutions, the proton-transfer rate at high temperatures, $T > 280$ K, is only slightly dependent on the temperature. To estimate the change in the activation energy as a function of temperature, we used a procedure we adopted from our previous work.[20] We fit the data of the Arrhenius plot by a polynomial (solid line in Figure 5) and then differentiated it. The activation energy obtained by this procedure is shown in Figure 6a for an H_2O solution and Figure 6c for an $MgCl_2$ 1 M solution. In general, the activation energy increases as the temperature decreases. For supercooled liquid water, the activation energy is much larger than at $T > 300$ K. In the ice phase, the activation energy is much larger than in the liquid phase, and it is almost temperature-independent. At a particular temperature T in pure water, the value of k_{PT} in the supercooled liquid is about twice as large as k_{PT} in ice at the same temperature (see Figure 5a). In $MgCl_2$ solutions, this large difference in k_{PT} in the liquid phase (and ice at the same temperature) decreases with the salt concentration. For large salt concentrations, 1.8 M $MgCl_2$, the value of k_{PT} in the liquid and solid phases at the freezing point ($T = 257$ K) is almost the same.

Proton Transfer in Ice. Figure 5b,c also shows an Arrhenius plot of the proton-transfer rate constant, k_{PT}, versus $1/T$ in the solid phase for different concentrations of $MgCl_2$ and NaCl. As seen in the figure, k_{PT} in ice strongly depends on the temperature. The value of the activation energy is almost constant, independent of the temperature or salt concentration. The activation energy of k_{PT} in pure water ice, found in this work and in our previous study,[20] is about the same $E_a \approx 30$ kJ/mol. In contrast, the activation energy of a salt solution is larger by a factor of 2 than that of pure water, 60 ± 8 kJ/mol. We estimate a 15% error in the activation energy determination. The error may arise from the fitting procedure, the proton-transfer model we use to fit the time-resolved emission data, the signal-to-noise ratio of the time-resolved emission, and the stability of the cryogenic temperature $\pm$ 1.5 K.

The recombination process is part of the photoacid protolytic cycle. In the time- resolved fluorescence of ROH in pure water and pure ice, the recombination of the proton to reform an excited photoacid is easily observed as a long-time nonexponential tail. In HPTS, the Coulomb attraction between the proton and the RO^- is large. In pure water, the distance in which the Coulomb attraction and the thermal energy are equal is about 28 Å. We used the Debye−Hückel screening potential given in eqs 3 and 4 in the model subsection to introduce the screening effect of the salt concentration on the recombination process. The screening depends on the square root of the salt concentration.

The ion screening decreases the Coulomb attraction between RO^- and the H^+ exponentially with the distance. As a consequence of the potential screening, the recombination is reduced, and the net result is that the time-resolved fluorescence of ROH decays almost exponentially for much longer times than in the pure water case in which the large Coulomb attraction causes a large increase in the recombination process. In pure water, the amplitude of the ROH emission long-time nonexponential tail is about 20% of the fluorescence peak at an early time. In a liquid salt solution of about 200 mM salt concentration, the amplitude of the long-time tail strongly decreases, and the long-time amplitude is less than 5%. In ice formed by fast cooling (about 10 °C/min) of a liquid salt solution down to a temperature below the freezing point, we find that the amplitude of the long-time tail in frozen solutions is small and comparable with that of a liquid solution of the particular sample. This fact indicates that the recombination process is also effectively low in the ice phase due to the Coulomb screening by the salt ions, and thus, the "salting out" process of the strong electrolyte is probably small. In the analysis of the ROH time-resolved emission of the ice samples, we use the Coulomb-screened

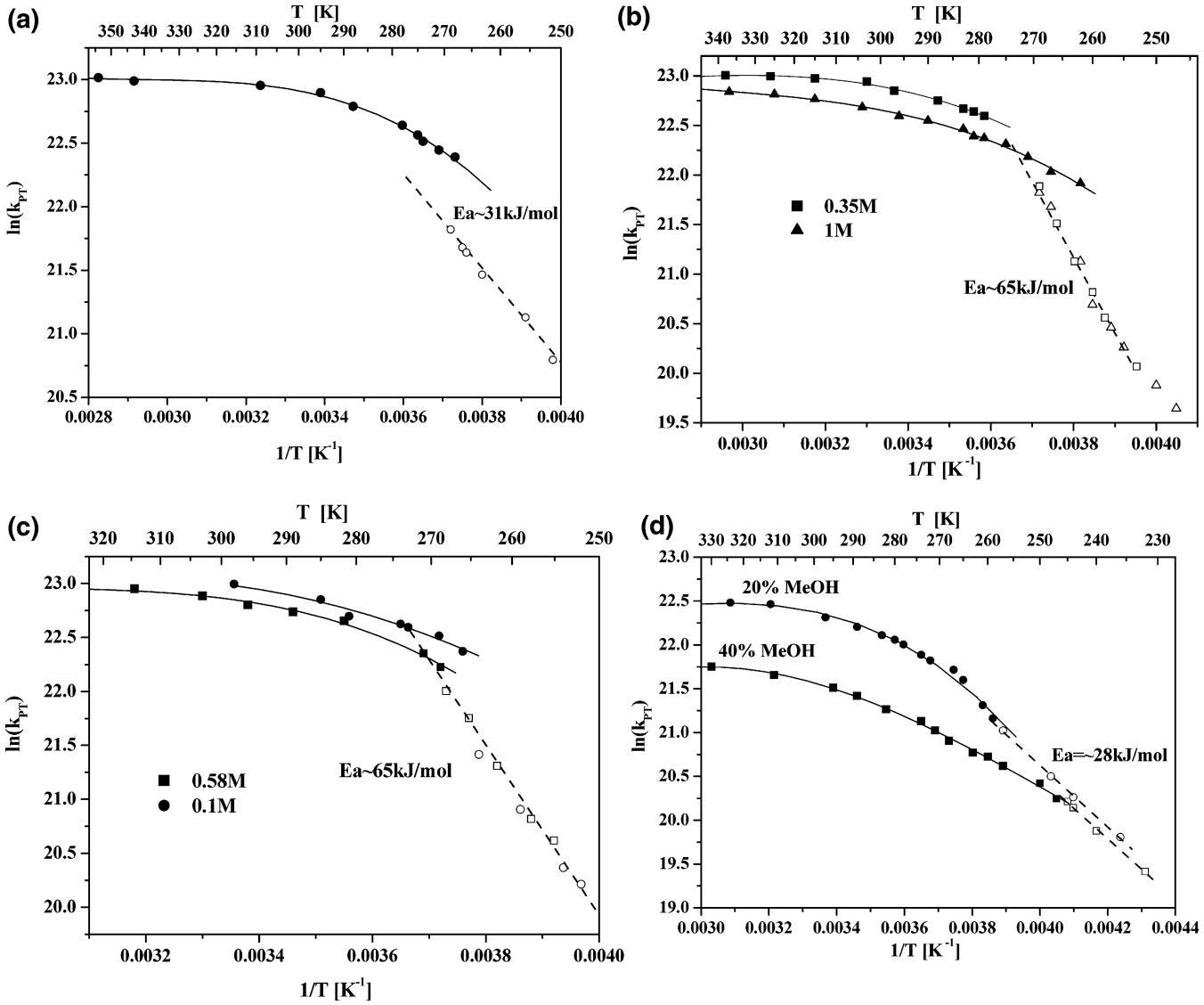

Figure 5. Arrhenius plot of the logarithm of the proton-transfer rate constant of HPTS in various solutions. Filled symbols, liquid phase; hollow symbols, solid state; solid line, polynomial fit to the liquid phase; broken line, linear fit to the ice phase. (a) H_2O. (b) $MgCl_2$ solutions. (c) NaCl solutions. (d) Water−methanol solutions.

potential with the same concentration as that introduced to the liquid solution (usually <1 M). The static dielectric constant of pure ice at about the freezing point is about $\epsilon_s = 100$. We are unaware of a published data of the values of $D(T)$ and $\epsilon_s(T)$ of the aqueous salt solutions and the water−methanol mixtures in the frozen phase. We therefore used a dielectric constant of $\epsilon_s = 100$ for the doped ice samples at all temperatures. We fit the time-resolved emission of the frozen salt solutions with our reversible geminate recombination model. The fits are good but not as good as in the liquid phase.

In ice, we noticed that a short-time component of about 200 ps exists in the ROH fluorescence decay, and we were unable to fit it by our model. This fast component may arise from early reactive steps of the complex multistaged proton-transfer process. In a previous study,[38] we adopted the framework of the model that was originally proposed by both Eigen[4] and Weller[3] for the intermolecular ESPT processes. The model extends the GR model to include an additional reactive step (Scheme 1).

The excited protonated acid ROH^* dissociates first to a contact ion pair, consisting of an anion and a hydrogen-bonded hydrated proton complex, which we designate H_3O^+. The contact ion pair $RO^{-*}\cdots H_3O^+$ exhibits about the same UV−vis spectroscopic signature as the RO^- emission band of the separated ion pair and the free RO^-. The extended model predicts that an additional short-time component will be present in the time-resolved emission of both ROH^* and RO^{-*}. In liquid water, we found that this component is ∼6 ps with an amplitude of about 0.25.[38] To account for the mismatch between the experimental data and the GR model, we introduce in the fit to the ROH fluorescence in ice an additional exponential component of $A \times \exp(-t/\tau)$, where $A \approx 0.2$ and $\tau = 0.2$ ns. The long-time tail amplitude depends on all the model parameters, which are as follows: τ and τ', the known lifetimes of ROH and RO^-, respectively; the unknown proton-transfer and recombination rate constants k_{PT} and k_r, the Coulomb potential, and the diffusion constant D. Since we do not know $\epsilon_s(T)$ and $D(T)$ in our frozen samples, as well as k_{PT} and k_r, we therefore use all these parameters as freely adjustable parameters. k_{PT}, the most important parameter in this study, is determined from the nearly exponential decay at early times. Unfortunately, the initial slope is also somewhat dependent on the recombination process. In both the liquid electrolyte solution and the solid phase, the Coulomb screening is large. The effect of the

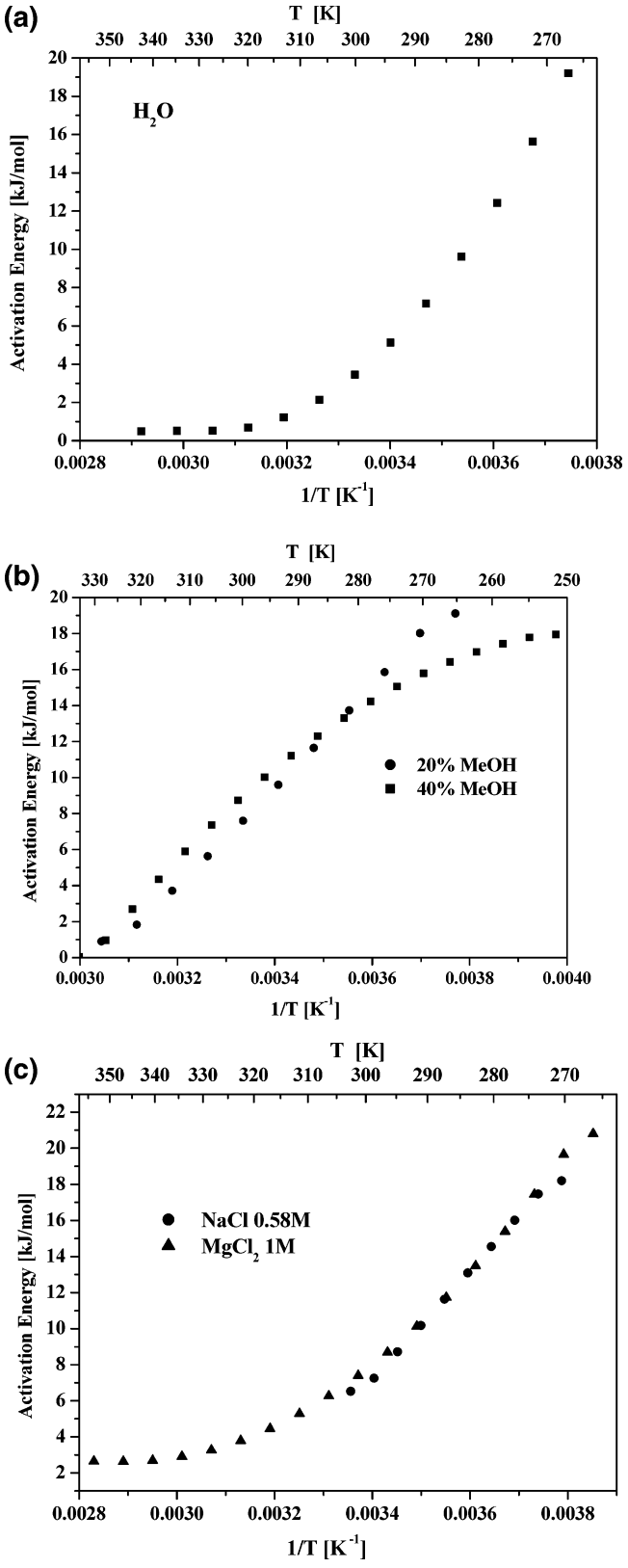

Figure 6. Activation energies of the proton-transfer reaction in liquid solutions derived by differentiation of the Arrhenius plots of Figure 5. (a) Water solutions. (b) Water−methanol solutions. (c) Water electrolyte solutions.

recombination process is small, and hence, the "destructive interference" of the recombination process on the determination of k_{PT} is small. Thus, we are quite confident that k_{PT} in a salt solution is measured with reasonable accuracy. We estimate the error in the determination of the k_{PT} to be 10%. The fitting parameters of HPTS in aqueous solution of 1 M $MgCl_2$ in the liquid−solid phases using the geminate recombination model and the values of D, as obtained from the best fit of the experimental data in pure ice, are given in Table 2. The fitting parameters in other salt solutions appear in the Supporting Information.

The values of proton diffusion in ice were measured in the 70's by Kelly and Salomon[39] and Camplin and Glen.[40] It was found that D_{H+} is smaller by about a factor of 2 than in the liquid at the freezing point, $D_{H+}^{ice} \approx 3.5 \times 10^{-5}$ cm^2/s. At the intermediate times, between the initial nearly exponential decay and the asymptotic $t^{-3/2}$ power law (0.1 ns $< t <$ 1 ns in pure water), k_r is the dominant parameter that determines the quality of the fit. The diffusion constant mainly affects the long-time fluorescence amplitude ($t >$ 1 ns in pure water). We used a value $D = 4 \times 10^{-5}$ cm^2/s in ice at the freezing point to obtain the best fit. We decreased the values $D(T)$ with the temperature decrease. The value of $\epsilon_s(T)$ was kept constant at all temperatures. As mentioned above, the Coulomb potential is strongly screened by the salt, and thus, the fluorescence long-time tail is much smaller than in pure ice.

Water−Methanol Mixtures. We measured the temperature dependence of the proton-transfer and recombination rate constants in water-rich water−methanol mixtures of $\chi_{CH_3OH} =$ 0.1 and 0.2. In a previous study,[41] we measured the photoprotolytic cycle of HPTS in water−methanol mixtures at room temperature. The proton-transfer and recombination rates strongly depend on the water−methanol composition. At room temperature, both k_{PT} and k_r decrease as the methanol mole fraction increases. In pure methanol, HPTS is incapable of transfering a proton within the excited-state lifetime, ($\tau_{PT} \gg \tau_f$). The dielectric constant and diffusion constant also depend on the composition. We were able to fit the time-resolved emission of both the ROH^* and RO^{-*} forms in these solutions in both the liquid and solid phases at all temperatures by the geminate recombination model. Figure 5d shows the Arrhenius plot of k_{PT} of HPTS in solutions of 0.1 and 0.2 mole fraction versus $1/T$.

As found in a pure water solution, at high temperatures, $T >$ 280 K, the value of the proton-transfer rate constant, k_{PT}, is almost independent of temperature, while at low temperatures, the dependence of k_{PT} on T increases as the temperature decreases. The samples of $\chi_{CH_3OH} = 0.1$ and 0.2 freeze at 261 and 243 K, respectively. In frozen water−methanol samples, the photo-protolytic cycle can be also fit with our geminate recombination model. In ice samples, the dielectric constant and the proton diffusion constant are unknown, and hence, we used them as freely adjustable parameters. At the freezing point, we used the values of ϵ_s and D of the liquid phase at the same temperature or at a slightly higher temperature. The parameters used to fit the ESPT process in a water−methanol mixture of $\chi_{CH_3OH} = 0.2$ are given in Table 3. The fitting parameters of water solution of $\chi_{CH_3OH} \approx 0.1$ is given in a table in the Supporting Information. We used the same differentiation procedure as in the salt samples to get the activation energy of the proton-transfer rate constant as a function of temperature in both the liquid and solid phases (see Figure 6b).

The temperature dependence of the activation energies of k_{PT} in the water−methanol liquid mixtures has some similarities with that of the pure water and water−salt solution. The activation energy depends on the temperature. The lower the temperature is, the larger the activation energy. The activation energy in the frozen sample is about 28 kJ/mol, slightly lower

SCHEME 1

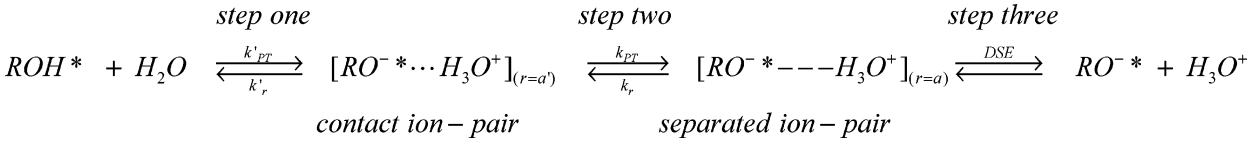

TABLE 3: Temperature Dependence of the Geminate Recombination Model Parameters for the Proton-Transfer Reaction of HPTS in a Methanol/H_2O ($\chi_{CH_3OH} = 0.2$) Solution

T [K]	k_{PT}[a] [10^9 s^{-1}]	k_r[a,b] [10^9 Å s^{-1}]	D[c] [cm^2 s^{-1}]
330	2.8	3.2	9.5×10^{-5}
311	2.7	3.2	6.8×10^{-5}
295	2.2	2.4	5.5×10^{-5} [e]
289	2.0	2.0	4.8×10^{-5}
282	1.72	1.6	4.3×10^{-5}
274	1.5	1.4	3.6×10^{-5}
271	1.35	1.1	3.1×10^{-5}
268	1.2	1.0	3.0×10^{-5}
263	1.05	1.0	2.9×10^{-5}
260	1.0	1.0	2.85×10^{-5}
257	0.90	0.95	2.8×10^{-5}
250	0.74	0.83	2.7×10^{-5}
247	0.62	0.64	2.6×10^{-5}
245[d]	0.60	0.64	2.6×10^{-5} [e]
244[d]	0.56	0.64	2.6×10^{-5} [e]
240[d]	0.43	0.51	2.0×10^{-5} [e]
232[d]	0.27	0.42	1.5×10^{-5} [e]

[a] k_{PT} and k_r are obtained from the fit of the experimental data by the reversible proton-transfer model (see text). [b] The error in the determination of k_r is 50%; see text. [c] Values obtained by best fit to the fluorescence decay. [d] Ice samples. [e] From water−methanol conductance measurement given by ref 33.

than that of pure water ($E_a \approx 30$ kJ/mol). It is smaller by a factor of 2 than that of k_{PT} of HPTS in salt-doped ice (60 kJ/mol).

Another interesting result concerns the values of the rate constant of proton-transfer k_{PT} at the freezing point in the liquid and that in the solid phase. The value of k_{PT} for pure water in the liquid phase is about twice that of the solid phase. In the liquid water−methanol mixture, the rate constants at the freezing point are about the same. We find that the activation energy of k_{PT} in the solid phase of solution $\chi_{CH_3OH} = 0.1$ and 0.2 mole fraction is about the same. Another interesting point is that the value of k_{PT} in the liquid phase of a water−methanol mixture of $\chi_{CH_3OH} = 0.2$ at the freezing point, 243 K, is close to the value of k_{PT} in the solid phase of the solution of $\chi_{CH_3OH} = 0.1$ (see Figure 5d).

Previous Model of the Temperature Dependence of the Proton-Transfer Rate Constant. Previously,[20,42,43] we used a qualitative model that accounts for the unusual temperature dependence of the excited-state proton transfer. The proton-transfer reaction depends on two coordinates. The first depends on a generalized solvent configuration. The solvent coordinate characteristic time is within the range of the dielectric relaxation time τ_D. The second coordinate is the actual proton translational motion along the reaction path.

The model restricts the proton-transfer process to a stepwise one. The proton moves to the adjacent hydrogen-bonded solvent molecule only when the solvent configuration brings the system to the crossing point according to the Kuznetsov model.[44] This simple model excludes parallel routes for the ESPT in which many solvent configurations permit the reaction to take place with a distribution of reaction rates, whereas in a two-dimensional model, these parallel routes are permitted and

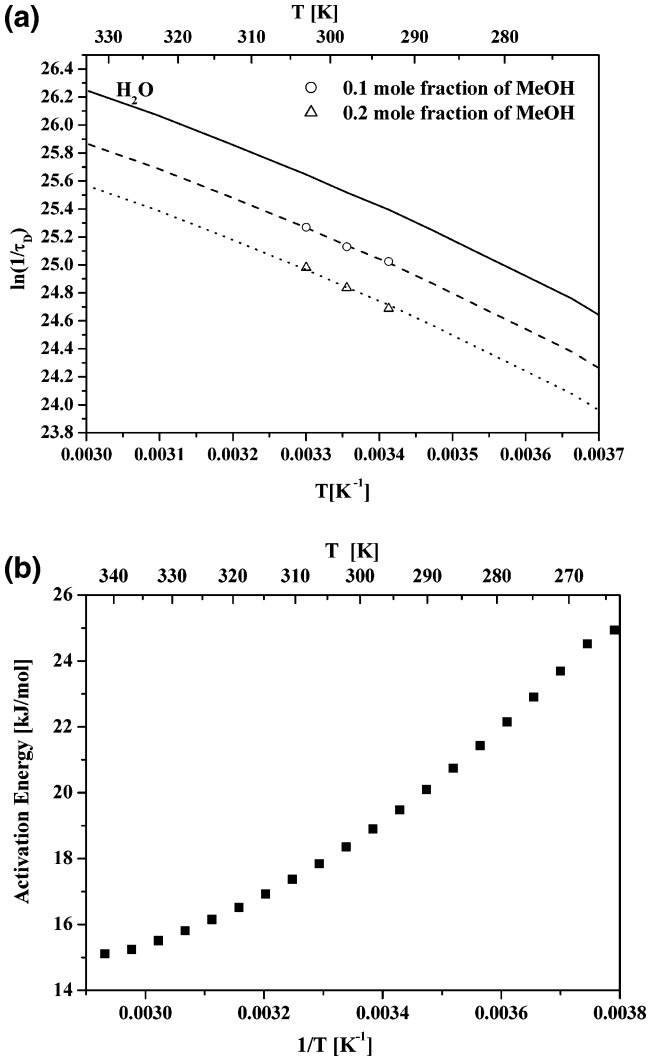

Figure 7. (a) Arrhenius plot of the inverse of the dielectric relaxation time, $1/\tau_D$ of pure water and water−methanol mixtures of 0.1 and 0.2 mol. Symbols data taken from refs 47 and 48. Solid line is polynomial fit. (b) Activation energy of the inverse of the water dielectric constant.

contribute to the overall effective rate. In the stepwise model, the overall proton-transfer time is a sum of two times, $\tau = \tau_1 + \tau_2$, where τ_1 is the characteristic time for the solvent reorganization, and τ_2 is the time for the proton to pass to the acceptor. The overall rate constant, $k_{PT}(T)$, at a given T is

$$k_{PT} = \frac{k_H(T)k_S(T)}{k_H(T) + k_S(T)} \tag{12}$$

where k_S is the solvent coordinate rate constant, and k_H is the proton coordinate rate constant.

Equation 12 provides the overall excited-state proton-transfer rate constant along the lines of a stepwise process similar to the processes mentioned above. As a solvent coordinate rate constant, we use $k_S(T) = b/\tau_D$, where b is an adjustable empirical factor determined from the computer fit of the experimental

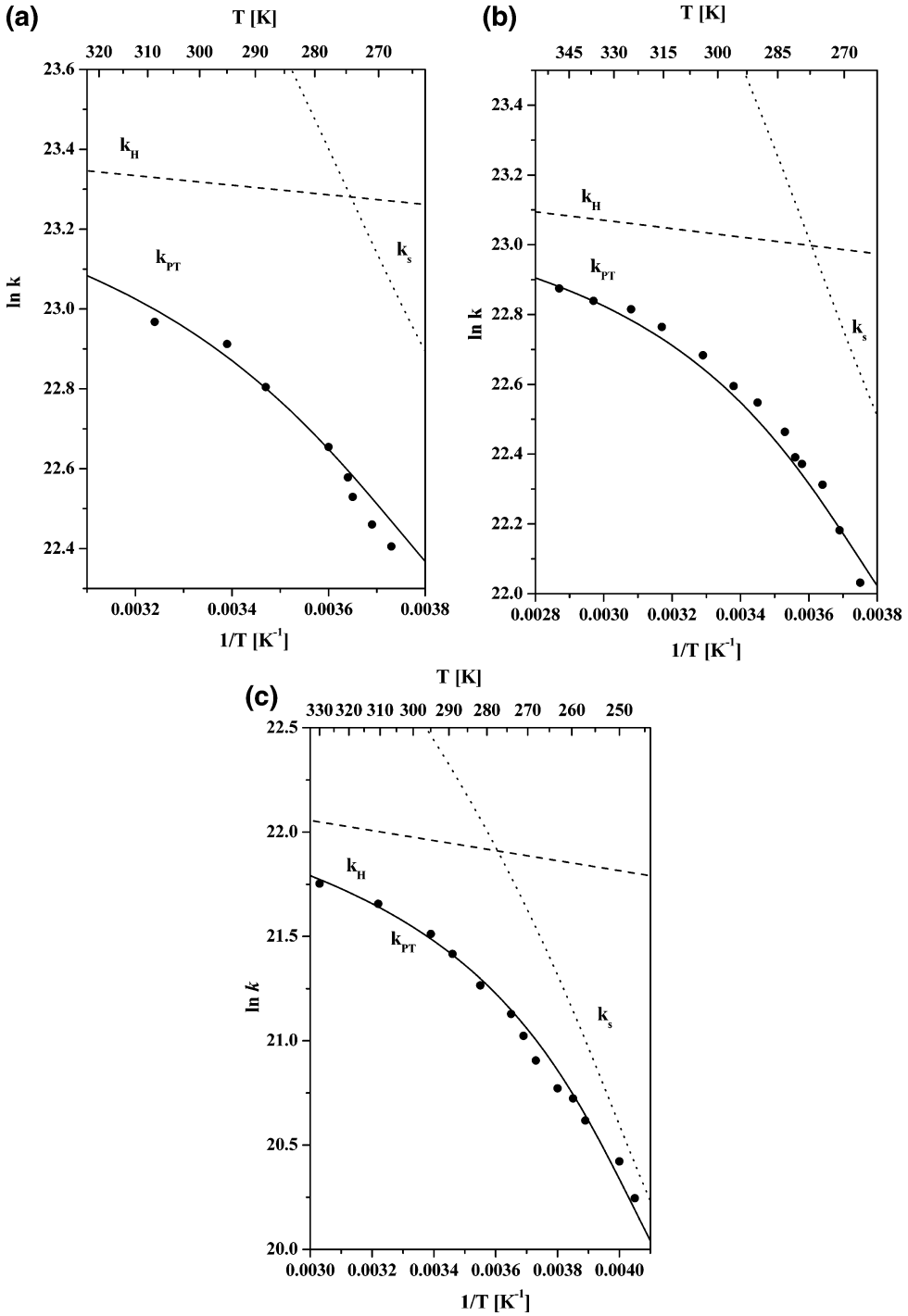

Figure 8. Fit by the stepwise model (solid line) to the Arrhenius plot of the experimental results of k_{PT}(symbols) in the liquid phase. Dotted line, the solvent relaxation rate constant $k_S(T)$; dashed line, the proton rate constant $k_H(T)$. (a) H_2O. (b) $MgCl_2$ 1 M. (c) Water−methanol mixture of $\chi_{CH_3OH} = 0.2$.

data. We previously found that the empirical factor depends on the photoacid and the solvent, and its value lies between 0.2 and 4. The reaction rate constant, k_H, along the proton coordinate is expressed by the usual activated chemical reaction description given by eq 13. For high temperatures, the solvent relaxation is fast, and the rate-determining step is the actual proton-transfer coordinate.

$$k_H = k_H^0 \exp\left(-\frac{\Delta G^{\ddagger}}{RT}\right) \tag{13}$$

where k_H^0 is the preexponential factor determined by the fit to the experimental results and $\Delta G^{\ddagger}$ is the activation energy.

The activation energy, $\Delta G^{\ddagger}$, is determined from the excited-state acid equilibrium constant, K_a^*, and the structure reactivity relation of Agmon and Levine.[45] K_a^* is calculated from the rate parameters derived from the time-resolved emission at the high limit temperature ~320 K, assuming that $k_H = k_{PT}$ according to

$$K_a^* = 10^{27} \frac{k_{PT}}{N_A k_a} \tag{14}$$

where N_A is Avogadro's number and $k_a = 4\pi a^2 k_r$.[46]

Figure 7a shows an Arrhenius plot of the inverse of the dielectric relaxation time, $1/\tau_D$, of pure water taken from ref 47

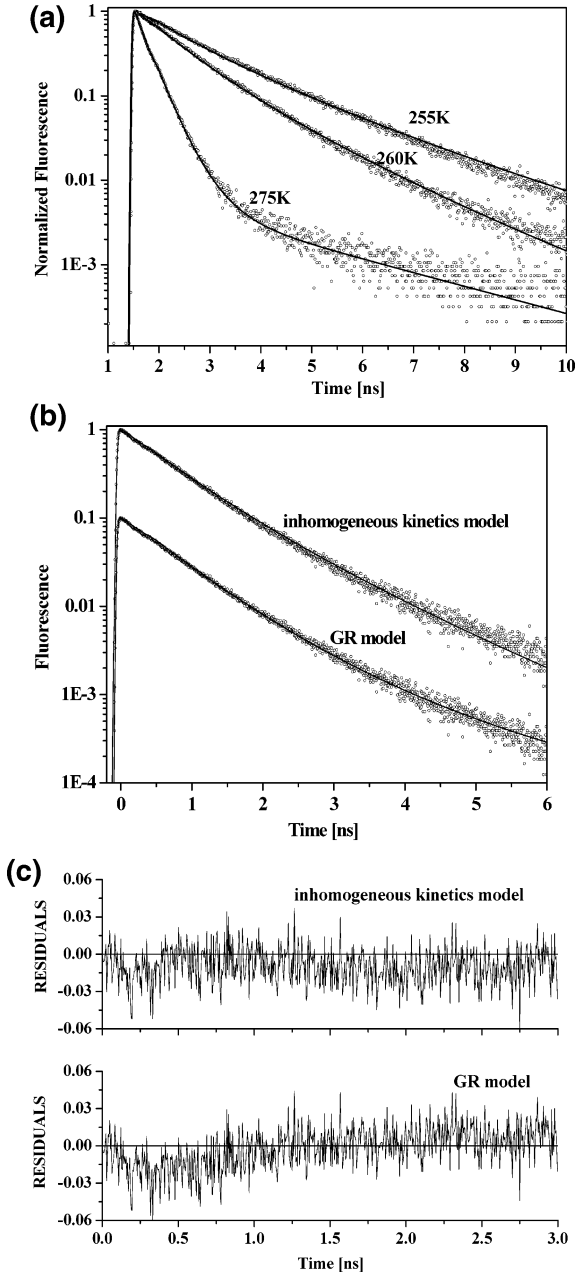

Figure 9. (a) Time-resolved emission at several temperatures of the ROH form of HPTS in the ice phase of an aqueous solution containing 1 M $MgCl_2$ (symbols) along with a fit using the inhomogeneous kinetics model (solid lines). **(**b) Same as (a), but the experimental data at $T =$ 262 K are fitted by two different models; see text. (c) The residuals of (b); note the better fit of the inhomogeneous model.

and for water−methanol mixtures of 0.1 and 0.2 mole fraction of methanol given at only three temperatures in ref 48. Figure 7b shows the activation energy of the inverse of the water dielectric constant calculated by the method described previously. The activation energy of $1/\tau_D$ at the high-temperature limit 330 K is about 15 kJ/mol, while at 270 K, it is about 25 kJ/mol. The activation energy at the high-temperature limit, 330 K, of k_{PT} of HPTS in pure water is much lower, $\leq$2 kJ/mol, while at low temperatures, it is about 20 kJ/mol, somewhat less than the activation energy of $1/\tau_D$ of cold water at about the same temperature.

Figure 4 in ref 20 shows the fit by the model described above of the Arrhenius plot of HPTS in pure water to the water dielectric relaxation time. Figure 8a−c shows the fit by this model (solid line) to the Arrhenius plot of the experimental results of k_{PT} (symbols) in the liquid phase of pure water, $MgCl_2$ 1 M solution, and the water−methanol mixture of $\chi_{CH_3OH} =$ 0.2, respectively. As seen in the figures, the quality of the fit is good at low temperatures and reasonable in the high-temperature range. We also plot the inverse of the dielectric relaxation time (dotted line), $k_S(T)$, and $k_H(T)$, the proton rate constant (dashed line).

TABLE 4: Temperature Dependence of Kinetic Parameters for the Proton-Transfer Reaction of HPTS in a 1 M $MgCl_2$ Using the Inhomogeneous Kinetic Model

T [K]	$K(x_0)$ [ns^{-1}]	$2\sigma^2$ (width)
262	5.80	0.37
260	4.50	0.48
257	3.20	0.56
255	2.60	0.67
250	1.90	0.91
247	1.50	1.33
242	1.15	2.86
239	1.05	3.33

Inhomogeneous Proton-Transfer Kinetics Model for Ice Samples. An inhomogeneous kinetics model accounts for a distribution of proton-transfer rates in disordered frozen water, which strongly affects the time-resolved emission of the ROH of a photoacid. We wish to use the model described in a separate subsection to fit the proton-transfer ice data. In ice, most of the water molecules are immobile. Only a few water molecules, at the defect point, can rotate.[35] We assume that the water next to the HPTS molecule or near an ion is in a frozen disordered structure.

Figure 9a shows the time-resolved emission at several temperatures of the ROH* form of HPTS in the ice phase of an aqueous solution containing 1 M $MgCl_2$. The fitting parameters of the inhomogeneous kinetic model are as follows: A, the preexponential in the rate constant expression (see eq 10); the width of the distribution, $2\sigma^2$; the position of the Gaussian population, x_0 (see eq 8). At $T =$ 262 K, we set the preexponential value to be 5.8×10^9 s^{-1}, while at $T =$ 242 K, $A =$ 1.15×10^9 s^{-1}.

The fitting parameters of the model change with the temperature and the phase (liquid or solid) of the solution. We set the parameter $x_0 = 1.5$ for all temperatures of the ice samples, since the temperature dependence is given in the preexponential parameter A (eq 9). The width of the distribution in liquid and solid samples distinctively changes. The width in ice at the freezing point is slightly larger than in the liquid state. The Gaussian width increases by a factor of about 9 from $2\sigma^2 =$ 0.3 in the liquid state to about 3 for low-temperature ice (239 K). The fitting parameters of the inhomogeneous kinetics model for the ice phase of a 1 M $MgCl_2$ aqueous solution is given in Table 4.

Figure 9b shows the experimental time-resolved emission of the ROH* of HPTS in 1 M $MgCl_2$ solution at 262 K in the ice phase along with the fits of two models used in this study. The upper curve (solid line) shows the inhomogeneous kinetics model fit, while the lower curve shows the fit by the geminate recombination model, (the curves are vertically shifted for clarity purpose). As seen in the figure, both models account for the complex nonexponential decay of ROH in ice. To get a better insight into which of the models fit better to the experimental results, we plot on Figure 9c the residuals of the two plots shown in Figure 9b. It is clearly seen that the inhomogeneous kinetics (IK) model fits better the ROH decay at the short and intermediate times of the first nanosecond. The residuals of the GR model deviate at this time range that overlaps $\tau_{PT} = 1/k_{PT}$.

Thus, the better fit of the IK model indicates that inhomogeneous kinetics indeed contributes to the complex decay of the ROH in ice.

In a previous study[20] on proton transfer in ice, we used a different model that accounts for the proton transfer, proton mobility, and geminate recombination. The model is based on diffusion-assisted chemical reaction formalism.[49,50] L-defects in ice[35] diffuse toward the excited molecule and react chemically whenever they encounter an excited molecule. The temperature dependence of the overall reaction rate constant arises from the temperature dependence of the L-defect concentration, L-defect mobility, and the intrinsic reaction rate constant at contact.

Summary

The reversible proton dissociation and geminate recombination of HPTS is studied as a function of temperature in water electrolyte solutions and binary water−methanol mixtures. The experimental data are analyzed by the reversible geminate recombination model. As found in a pure water solution, at high temperatures, $T > 280$ K, the value of the proton-transfer rate constant, k_{PT} , is almost independent of temperature (small activation energy), while at low temperatures, the dependence of k_{PT} on T increases as the temperature decreases (the activation energy increases as the temperature decreases; see Figure 6). In the solid phase, the Arrhenius plot of $\ln(k_{PT})$ versus $1/T$ is nearly constant, and the activation energy of the proton transfer of an electrolyte solution is large, $E_a \approx 60$ kJ/mol, while the activation energy of the proton-transfer rate in the solid phase of the water−methanol mixtures is somewhat lower than in pure water, $E_a \approx 28$ kJ/mol. Careful examination of the time-resolved emission in ice samples shows that the fit quality using the geminate recombination model is rather poor at short times. We were able to get a better fit using an inhomogeneous kinetics model assuming the proton-transfer rate consists of a distribution of rates. The model is consistent with an inhomogeneous frozen water distribution next to the photoacid.

In salt solutions, in both the liquid and ice phases, we find a large reduction of the geminate recombination because of the Coulomb attraction screening by the salt between the transferred proton and the basic form RO^- that is fourfold negatively charged. In the methanol−water solution, at all temperatures, the proton-transfer and recombination rate constants are smaller than in the pure water solution at the same temperatures. In addition, the overall recombination process is enhanced because both the dielectric and diffusion constants in the water−methanol solvent mixture are smaller than those in pure water.

Acknowledgment. We thank Prof. N. Agmon for his helpful and fruitful suggestions and discussions. This work was supported by grants from the Binational US-Israel Science Foundation and the James-Franck German-Israel Program in Laser-Matter Interaction.

Supporting Information Available: The kinetic parameters for the fit of the experimental time-resolved emission of HPTS in several solutions using the geminate recombination model are given in several tables. This material is available free of charge via the Internet at http://pubs.acs.org.

References and Notes

(1) Bell, R. P. *The Proton in Chemistry*, 2nd ed.; Chapman and Hall: London, 1973.

(2) *Proton Transfer Reaction*; Caldin, E. F., Gold, V., Eds.; Chapman and Hall: London, 1975.

(3) (a) Weller, A. *Prog. React. Kinet.* **1961**, *1*, 189, (b) *Z. Phys. Chem.* **1958**, N.F., *15*, 438.

(4) (a) Eigen, M. *Angew. Chem., Int. Ed.* **1964**, *3*, 1. (b) Eigen M.; Kruse W.; Maass G.; De Maeyer, L. *Prog. React. Kinet*. **1964**, *2*, 285.

(5) Ireland, J. E.; Wyatt, P. A. *Adv. Phys. Org. Chem*. **1976**, *12*, 131.

(6) (a) Gutman, M.; Nachliel, E. *Biochem. Biophys. Acta* **1990**, *391*, 1015. (b) Pines, E.; Huppert, D. *J. Phys. Chem.* **1983**, *87*, 4471.

(7) Kosower, E. M.; Huppert, D.; *Annu. Rev. Phys. Chem*. **1986**, *37*, 127.

(8) Tolbert, L. M.; Solntsev, K. M. *Acc. Chem. Res.* **2002**, *35*, 1.

(9) (a) Rini, M.; Magnes, B. Z.; Pines, E.; Nibbering, E. T. J. *Science* **2003**, *301*, 349. (b) Mohammed, O. F.; Pines, D.; Dreyer, J.; Pines, E.; Nibbering, E. T. J. *Science* **2005**, *310*, 5745.

(10) Prayer, C.; Gustavsson, T.; Tarn-Thi, T. H. In *Fast Elementary Processes in Chemical and Biological Systems*; 54th International Meeting of Physical Chemistry; AIP: New York, 1996; p 333.

(11) Tran-Thi, T. H.; Gustavsson, T.; Prayer, C.; Pommeret, S.; Hynes, J. T. *Chem. Phys. Lett*. **2000**, *329*, 421.

(12) Agmon, N. *J. Phys. Chem. A* **2005**, *109*, 13.

(13) Smith, K. K; Huppert, D.; Gutman, M.; Kaufmann, K. *J. Chem. Phys. Lett*. **1979**, *64*, 22.

(14) Clark, J. H.; Shapiro, S. L.; Campillo, A. J.; Winn, K. J. *J. Am Chem. Soc*. **1979**, *101*, 746.

(15) Politi, M. J.; Fendler, J. H. *J. Am. Chem. Soc*. **1984**, *106*, 265.

(16) Pines, E.; Huppert, D. *J. Chem. Phys*. **1986**, *84*, 3576.

(17) Pines, E.; Huppert, D.; Agmon, N. *J. Chem. Phys*. **1988**, *88*, 5620.

(18) Huppert, D.; Kolodney, E.; Gutman, M.; Nachliel, E. *J. Am. Chem. Soc.* **1982**, *104*, 6949.

(19) Leiderman, P.; Gepshtein, R.; Uritski, A.; Genosar, L.; Huppert, D. *J. Phys. Chem*. **2006**, *110*, 5573.

(20) Poles, E.; Cohen, B.; Huppert, D. *Isr. J. Chem.* **1999**, *39*, 347.

(21) *Handbook of Chemistry and Physic*s, 66th ed.; Weast, R. C., Astle, M. J., Eds; CRC Press: Boca Raton, FL, 1985.

(22) Robinson, R. A.; Stokes R. H. *Electrolyte Solutions*, 2nd ed.; Butterworth: London, 1959; Appendices 1.1 and 6.2.

(23) Rice, S. A. In *Diffusion-Limited Reactions*; Bamford, C. H., Tipper, C. F. H., Compton, R. G., Eds.; Comparative Chemical Kinetics, Vol. 25; Elsevier: Amsterdam, 1985.

(24) Agmon, N. *J. Chem. Phys.* **1984**, *81*, 2811.

(25) Agmon, N.; Goldberg, S. Y.; Huppert, D. *J. Mol. Liq.* **1995**, *64*, 161.

(26) Krissinel, E. B.; Agmon, N. *J. Comput. Chem.* **1996**, *17*, 1085.

(27) Lewis, G. N.; Doody, T. C. *J. Am. Chem. Soc*. **1993**, *55*, 3504.

(28) Haar, H. P.; Klein, U. K. A; Hfiner, F. W.; Hauser, M. *Chem. Phys. Lett.* **1977**, *49*, 416.

(29) Timmerman, J. *Physico-Chemical Constants of Binary Systems*; Interscience: 1960; Vol. 4.

(30) Erdey-Gruz, T.; Lengyel, S. In *Modern Aspects of Electrochemistry*; Bockris, J. O'M., Conway, B. E., Eds.; Battherworths: New York, 1964; Vol. 12, pp 1−40.

(31) Cornish, B. D.; Speedy, R. J. *J. Phys. Chem.* **1984**, *88*, 1888.

(32) Heise, V. R. *Z. Naturf.* **1958**, *13a*, 547.

(33) Erdey-Gruz, T.; Kugler, E. *Magyar Kemiai Folyoirat* (in Hungarian) **1968**, *74*, 135.

(34) Gepshtein, R.; Huppert, D.; Agmon, N. *J. Phys. Chem*. **2006**, *110*, 4434.

(35) Hobes, P. V. *Ice Physics*; Clarendon Press: Oxford, 1974.

(36) Gepshtein, R.; Leiderman, P.; Genosar, L.; Huppert, D. *J. Chem. Phys*. **2005**, *109*, 9674.

(37) Hasted, J. B.; Ritson, D. M.; Collie, C. H. *J. Chem. Phys*. **1948**, *16*, 1−21.

(38) Leiderman, P.; Genosar, L.; Huppert, D. *J. Phys. Chem. A* **2005**, *109*, 5965.

(39) Kelly,I. J.; Salomon, R. R. *J. Phys. Chem.* **1969**, *50*, 75.

(40) Camplin, G. C.; Glen, J. W. In *Physics and Chemistry of Ice*; Whalley, E., Jones, S. J., Gold, L. W., Eds.; Royal Society of Canada: Ottawa, 1973; p 256.

(41) Huppert, D.; Goldberg, S. Y.; Masad, M.; Agmon, N. *Phys. Rev. Lett.* **1992**, *68*, 3932.

(42) Cohen, B.; Huppert, D. *J. Phys. Chem. A* **2001**, *105*, 2980.

(43) Cohen, B.; Leiderman, P.; Huppert, D. *J. Phys. Chem. A* **2002**, *106*, 11115.

(44) German, E. D.; Kuznetsov, A. M.; Dogonadze, R. R. *J. Chem. Soc., Faraday Trans. 2* **1980**, *76*, 1128.

(45) Agmon, N.; Levine, R. D. *Chem. Phys. Lett.* **1977**, *52*, 197.

(46) Cohen, B.; Huppert, D. *J. Phys. Chem. A* **2000**, *104*, 2663.

(47) Kattze, U. J. *Chem. Eng.* **1989**, *34*, 374.

(48) Sato. T. *J. Chem. Phys*. **2000**, *112*, 2924.

(49) Szabo, A. *J. Phys. Chem.* **1989**, *93*, 6929.

(50) Collins, F. C.; Kimball, G. E. *J. Colloid Sci.* **1949**, *4*, 425.